Imaging Neuronal Seal Resistance on Silicon Chip using Fluorescent Voltage-Sensitive Dye

Dieter Braun and Peter Fromherz
Department of Membrane and Neurophysics, Max Planck Institute for Biochemistry, Martinsried/Munich, Germany

ABSTRACT The electrical sheet resistance between living cells grown on planar electronic contacts of semiconductors or metals is a crucial parameter for bioelectronic devices. It determines the strength of electrical signal transduction from cells to chips and from chips to cells. We measured the sheet resistance by applying AC voltage to oxidized silicon chips and by imaging the voltage change across the attached cell membrane with a fluorescent voltage-sensitive dye. The phase map of voltage change was fitted with a planar core-coat conductor model using the sheet resistance as a free parameter. For nerve cells from rat brain on polylysine as well as for HEK293 cells and MDCK cells on fibronectin we find a similar sheet resistance of 10 MΩ. Taking into account the independently measured distance of 50 nm between chip and membrane for these cells, we obtain a specific resistance of 50 Ωcm that is indistinguishable from bulk electrolyte. On the other hand, the sheet resistance for erythrocytes on polylysine is far higher, at ~1.5 GΩ. Considering the distance of 10 nm, the specific resistance in the narrow cleft is enhanced to 1500 Ωcm. We find this novel optical method to be a convenient tool to optimize the interface between cells and chips for bioelectronic devices.

INTRODUCTION

Noninvasive interfacing of neurons enables both long-term neurophysiological measurements and neuroprosthetic interfaces. Various approaches with planar metal electrodes have been pursued (Gross, 1979; Pine, 1980; Thomas et al., 1972; Regehr et al., 1988). Neurons were also coupled to electrically insulated semiconductors (Fromherz et al., 1991; Fromherz and Stett, 1995) which offer an interfacing without electrochemical currents that may damage electrodes and cells. Crucial for the strength of coupling between neurons and insulated silicon or metallic contacts is the seal resistance. It is determined by the thin sheet of electrolyte between cell membrane and oxidized silicon. This sheet of electrolyte together with the adjacent insulating films of membrane and oxide define a planar core-coat conductor that is open at its periphery to the bath (Weis et al., 1996; see also this article, Fig. 1 *a*). The sheet resistance and the capacitance of membrane and silicon oxide determine the electrical coupling between cells and chip in both directions—for stimulation and for detection of neuronal excitation.

Here we present an optical method to image the electrical characteristics of cell-silicon junctions. The cell is stimulated by a periodic voltage between silicon and bath. A membrane-bound dye (Fig. 1 *b*) probes the resulting voltage across the cell membrane. The fluorescence signal is acquired at high resolution in space and time with a confocal microscope using a lock-in technique (Fig. 1 *c*) and evaluated in terms of a two-dimensional core-coat conductor model. The approach reveals microscopic details as opposed to impedance measurements of cells on metal electrodes (Giaever and Keese, 1991; Lo and Ferrier, 1998; Wegener et al., 2000) which allows to infer only global electrical properties of confluent cell layers with ambiguous interpretation of the seal resistance. We use fluorescent amphiphilic dyes which are well established to record voltage transients in neurons at low to medium resolution (Cohen and Salzberg, 1978; Fluhler et al., 1985; Grinvald et al., 1983; Gross et al., 1986; Hibino et al., 1991; Meyer et al., 1997; Rohr and Salzberg, 1994; Windisch et al., 1995). We show how a lock-in approach can image cellular response maps at the limit of optical resolution in three dimensions.

Voltage in cell-solid junction

We consider a cell on an electrically conductive solid with no Faradayic current across the solid-electrolyte interface (Fig. 1 *a*). Cell membrane and solid/electrolyte interface have area-specific capacitances c_M and c_S. We assume that the cleft between cell and substrate has a constant sheet resistance r_J and a constant width d_J, small compared to the diameter of the junction, with a negligible transition region at the periphery (Braun and Fromherz, 1998). The cell-silicon contact is a planar core-coat conductor. Ionic conductances of the membrane can be neglected for intact cells with closed ion channels (Weis and Fromherz, 1997). We apply a changing electrical potential $V_S(t)$ to the substrate with the bulk electrolyte at constant potential $V_E = const$. The junction reacts with a potential profile $V_J(x,y,t)$ and the cytoplasm with a potential $V_M(t)$. This gives rise to voltages V_M–V_J and V_M–V_E across attached and free membrane.

Submitted January 15, 2004, and accepted for publication April 1, 2004.

Address reprint requests to Peter Fromherz, Dept. of Membrane and Neurophysics, Max Planck Institute for Biochemistry, Martinsried/Munich, Germany 82152. E-mail: fromherz@biochem.mpg.de.

Dieter Braun's present address is Biophysics Department, Ludwig Maximilians University, Munich, Germany 80799.

0006-3495/04/08/1351/09 $2.00

doi: 10.1529/biophysj.104.039990

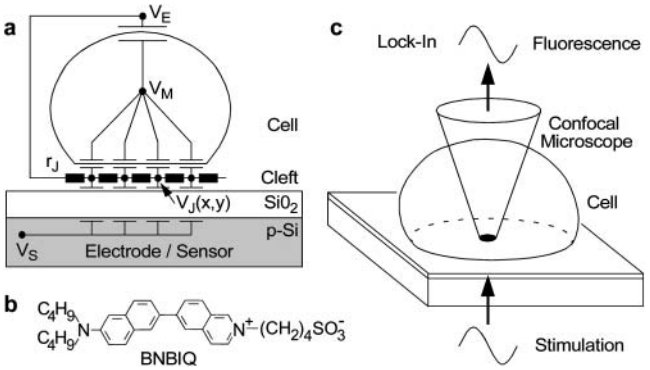

FIGURE 1 Electro-optical imaging of cell-electrode coupling. (*a*) Core-coat conductor model of cell-electrode junction. A cell is in contact with oxidized silicon through a narrow cleft (radius ~10 μm, height ~50 nm), characterized by a sheet resistance r_J. The solid insulation and the cell membrane are characterized by area-specific capacitances c_M and c_S. A sinusoidal modulation of the solid potential V_S against an external potential V_E of bulk electrolyte gives rise to a potential profile $V_J(x,y)$ in the junction together with an intracellular potential V_M. Voltage-sensitive dye molecules probe the voltages V_M–V_J and V_M–V_E across attached and free membrane. (*b*) Amphiphilic hemicyanine dye BNBIQ. (*c*) Electro-optical imaging. A lock-in method records the relative changes of fluorescence $\Delta F/F$ in the attached and the free membrane in amplitude and phase using a confocal microscope.

Plate contact model

The balance of current in each area element of the junction is symbolized by the circuit of Fig. 1 *a*. The current along the cleft and through the attached membrane is driven by capacitive stimulation from the solid (Eq. 1). In the cell, the current through the total attached membrane is balanced by the current through the free membrane according to Eq. 2, where $\langle V_J\rangle$ is the spatially averaged potential in the junction and $\beta_M = A_{JM}/A_{FM}$ is the ratio of attached and free membrane area.

$$-\nabla\left(\frac{1}{r_J}\nabla V_J\right) + c_M\frac{\partial(V_J - V_M)}{\partial t} = c_S\frac{\partial(V_S - V_J)}{\partial t}. \quad (1)$$

$$\frac{d(\langle V_J\rangle - V_M)}{dt} = \frac{1}{\beta_M}\frac{d(V_M - V_E)}{dt}. \quad (2)$$

We substitute $V_M(t)$ and obtain Eq. 3 with an effective area-specific capacitance of the cell $\tilde{c}_M = c_M/(1+\beta_M)$. The left-hand side describes the diffusion of charge along the core-coat conductor and the right-hand side accounts for nonlocal coupling by the cytoplasm and for capacitive stimulation. The boundary condition is $V_J(x,y,t) = V_E$ at the periphery of the attached membrane.

$$-\nabla\left(\frac{1}{r_J}\nabla V_J\right) + (c_S + \tilde{c}_M)\frac{\partial(V_J - V_E)}{\partial t} = \beta_M\,\tilde{c}_M\frac{\partial(\langle V_J\rangle - V_J)}{\partial t} + c_S\frac{d(V_S - V_E)}{dt}. \quad (3)$$

Time constant

We disregard the nonlocal coupling in Eq. 3 by replacing the average with the local potential $\langle V_J\rangle = V_J$ and assume a circular contact of radius a_J. After a voltage step $dV_S/dt = V_S^0\delta(t)$ we find a leading term $V_J(t) \propto \exp(-t/\tau_J)$ with a characteristic time constant $\tau_J = (c_S+\tilde{c}_M)r_J/\alpha_1^2$, where $(\alpha_1 a_J)^2 = 5.783$ is defined by the first zero of the Bessel function J_0 $(\alpha_1 a_J) = 0$ (Crank, 1975). We use τ_J and its related frequency f_J for global characterizations of junctions of area A_{JM} according to Eq. 4:

$$\tau_J = \frac{1}{2\pi f_J} = \frac{r_J(c_S + \tilde{c}_M)\,A_{JM}}{5.783\pi}. \quad (4)$$

AC stimulation

For sinusoidal stimulation with a frequency f we consider the complex Fourier amplitudes $\underline{V}_J$ and $\underline{V}_S$. From Eq. 3 we obtain for the transfer function $\underline{h}_J = (\underline{V}_J–\underline{V}_E)/(\underline{V}_S–\underline{V}_E)$:

$$-\frac{1}{2\pi i f}\nabla\left(\frac{1}{r_J}\nabla\underline{h}_J\right) + (c_S + c_M)\underline{h}_J = \beta_M\,\tilde{c}_M\langle\underline{h}_J\rangle + c_S. \quad (5)$$

We solve it for two dimensions with boundary condition $h_J = 0$ by an overrelaxation algorithm. The transfer functions between chip stimulation and free and attached membrane are defined by $\underline{h}_{FM} = (\underline{V}_M–\underline{V}_E)/(\underline{V}_S–\underline{V}_E)$ and $\underline{h}_{JM} = (\underline{V}_M–\underline{V}_J)/(\underline{V}_S–\underline{V}_E)$. They are obtained as $\underline{h}_{FM} = \langle\underline{h}_J\rangle\,\beta_M/(1+\beta_M)$ and $\underline{h}_{JM} = \underline{h}_{FM} - \underline{h}_J$. For illustration, they were calculated for a circular junction of radius a_J using $c_S/c_M = 0.33$ and $\beta_M = 0.5$. Fig. 2 shows radial amplitude and phase profiles of $\underline{h}_{JM}$ (a/a_J) along with $\underline{h}_{FM}$ in the surrounding for six relative frequencies f/f_J.

At low frequencies, the junction is dominated by the cleft resistance in series to the chip capacitor, yielding a phase shift of $-90°$ for the attached membrane and $+90°$ for the free membrane (Fig. 2 *a*). At high frequencies, the cell capacitance dominates with a phase shift of $-180°$ for the attached membrane and no phase shift for the free membrane. In both limits, the phase profile in the junction is rather flat with a jump to the level of the free membrane near the periphery at $a/a_J = 1$. In an intermediate frequency range $f/f_J \sim 1$ there is a shallow phase trough across the junction. The phase profile is shifted from $-90°$ toward $-180°$ with increasing frequency. The amplitudes at high frequency are $|h_{JM}^\infty| = 0.22$ and $|h_{FM}^\infty| = 0.11$, determined by the capacitive voltage divider. At intermediate frequencies $f/f_J \sim 1$ there is a distinct cupola of the amplitude in the junction with a narrow minimum near the periphery.

MATERIALS AND METHODS

Stimulation chips

Stimulation chips were optimized for high capacitance, response times below 1 μs, and high fluorescence intensity. The fabrication of chip type A

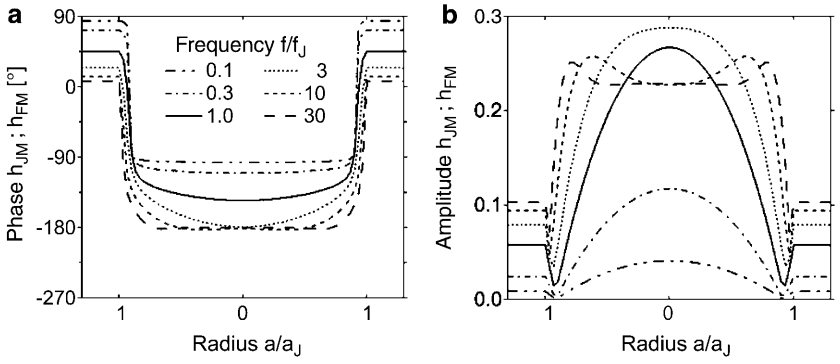

FIGURE 2 Theoretical AC response of circular cell-electrode junction. (*a*) Phase and (*b*) amplitude of the complex valued transfer function $\underline{h}_{JM} = (\underline{V}_M - \underline{V}_J)/(\underline{V}_S - \underline{V}_E)$ from electrode to the attached cell membrane is plotted versus the scaled radial coordinate a/a_J at different scaled frequencies f/f_J. Beyond the periphery $a/a_J > 1$, the transfer function $\underline{h}_{FM} = (\underline{V}_M - \underline{V}_E)/(\underline{V}_S - \underline{V}_E)$ from electrode to the free cell membrane is shown. The characteristic frequency f_J marks the highpass filter onset for a circular cell-electrode coupling.

was described previously (Braun and Fromherz, 2001). For chip type B, we used highly p-doped silicon wafers (4" diameter, 400 μm thickness, 100 crystal surface, polished one side, 2–4 m, Ωcm, Aurel, Landsberg, Germany). A field oxide of 1070 nm was grown. A circular stimulation spot (diameter 500 μm) was opened on the front side and covered with 16 nm or 50 nm silicon oxide. The back of the chip was contacted by 200 nm chromium. Chips were cut to octagons of 4 mm diameter and attached to 35-mm plastic dishes (Falcon 3001, Becton-Dickinson, Heidelberg, Germany) with a silicone glue (MK3, Sulzer Medica, Köln, Germany).

Cells

Erythrocyte ghosts were prepared according to a protocol of Schwoch and Passow (1973), as described previously (Braun and Fromherz, 1997). Chips were wiped with a detergent (2% Tickopur RP100, Bandelin, Berlin, Germany) at 60°C, rinsed with Milli-Q water (Millipore, Billerica, MA), dried with nitrogen and sterilized by ultraviolet (30 min). Several hours before the measurement a solution of 0.5 mg/ml poly-L-lysine (MW 10,000, Sigma, Heidelberg, Germany) in TRIS buffer was applied and rinsed three times with TRIS buffer. Human embryonic kidney (HEK293) cells (Graham et al., 1977) were obtained from ATCC (Manassas, VA; CRL-1573). Before culturing, cleaned chips were coated with fibronectin (Sigma, 25 μg/ml in PBS overnight) or poly-L-lysine (Sigma, MW 10,000, 100 μg/ml in PBS overnight). Trypsinated cells were cultured on the chips for 2–3 days at 37°C in 5% CO_2 to a confluency of 50% in 3 ml medium (13.9 mg/ml DMEM (074-02100A, Gibco, Invitrogen, Karlsruhe, Germany) with 10% heat-inactivated fetal bovine serum (FBS, Seromed, Berlin, Germany), 3.7 mg/ml $NaHCO_3$ (Sigma), 4 mM L-glutamine, 25 U/ml penicillin and streptomycin (Gibco) at pH 6.8. Madine Darby Canine Kidney (MDCK) cells were obtained from European Collection of Cell Cultures (Cambridge, UK; 85011435). The cleaned chips were coated with poly-L-lysine (Sigma, MW 10000, 100 μg/ml in PBS overnight). Trypsinated cells were cultured on the chips in EMEM (21885-025, Gibco) with 2 mM glutamine, 1% non-essential amino acids (11140-035, Gibco), and 10% fetal bovine serum (10270098, Gibco). Other treatments were identical to HEK cells. Culturing neurons from embryonic rat brain followed previously described protocols (Banker and Cowan, 1977; Vassanelli and Fromherz, 1999).

Voltage-sensitive dye

We used the amphiphilic hemicyanine dye dibutylamino-naphtalene-butylsulfonato-isoquinolinium, i.e., BNBIQ (this article, Fig. 1 *b*; see also Ephardt and Fromherz, 1993). Voltage-sensitive fluorescence in a cell membrane is due to identical spectral shifts of excitation and emission that are caused by interaction of the electrical field with intramolecular charge-displacement (Kuhn and Fromherz, 2003). The response time of fluorescence changes induced by such a molecular Stark effect is limited by the fluorescence lifetime which is in a range of 1 ns (Röcker et al., 1996). The relative change of fluorescence intensity F is proportional to a change of transmembrane voltage as $\Delta F/F = S_{DYE}\ \Delta V_M$ with a sensitivity $S_{DYE} \approx -10\%/100$ mV in leech neurons (Fromherz and Müller, 1993; Kuhn and Fromherz, 2003). We prepared a saturated dye solution in a 1:1 mixture of fetal bovine serum and Milli-Q water and added 40 μl to the culture medium. The experiments started after a few minutes to avoid internalization of the dye.

Stimulation

The bath was contacted with a 3 × 30 mm platinum electrode. An AC voltage from a function generator (model 33120A, Hewlett-Packard, Böblingen, Germany) with an amplitude $\underline{V}^0_{STIM}$ was applied to the chip against the bath potential. It was superposed by a DC bias to the chip of 1 V + 2 $\underline{V}^0_{STIM}$. The frequency was chosen near the presumed characteristic frequency f_J. In some experiments we applied a train of rectangular voltage pulses with an amplitude of $\underline{V}^0_{STIM} = -6$ V, a chip bias of +7 V, and a pulse duration of 4 μs.

Fluorescence

A confocal microscope (FluoView 1.26, Olympus, Hamburg, Germany) was used to achieve optical recording in three dimensions. We used a water objective (UApo/340, $NA = 1.15$, 40×) with built-in coverslip and no plan correction. On the basis of the spectral sensitivity of BNBIQ (Kuhn and Fromherz, 2003) we used an excitation at 488 nm (Ar laser, Stabilite 2017, Spectra Physics, Irvine, CA) and an emission filter between 590 and 700 nm (AHF, Tübingen, Germany). Fluorescence was detected with a photomultiplier (R928, Hamamatsu, Bridgewater, NJ; built-in amplifier, Olympus) and sampled at 5 MHz with 12 bits (PCI 6110E, National Instruments, Austin, TX). For each pixel we correlated the photomultiplier signal V_{PM} to the stimulation voltage V_{STIM} using a lock-in algorithm. The in-phase and out-of-phase amplitudes V_x, V_y were obtained from the scalar product of the time average according to Eq. 6 with the appropriate phase of the reference V_{STIM}.

$$V_{x,y} = \sqrt{2}\frac{\langle V_{PM}\, V_{STIM}\rangle - \langle V_{PM}\rangle\langle V_{STIM}\rangle}{\sqrt{\langle V_{STIM}\, V_{STIM}\rangle - \langle V_{STIM}\rangle\langle V_{STIM}\rangle}}. \qquad (6)$$

The complex relative signal $\underline{V}_{PM}/\overline{V}_{PM}$ was defined by $\underline{V}_{PM} = V_x + iV_y$ and $\overline{V}_{PM} = \langle V_{PM}\rangle - \langle V_{back}\rangle$ with background $\langle V_{back}\rangle$. A typical scan included 64 × 64 pixels, with a dwell time of 4 ms per pixel to limit bleaching and phototoxic effects. 100 to 500 periods were considered at frequencies $f = 25$–125 kHz. The signal/noise ratio was ~3%. It was further reduced by binning several pixels.

Phase corrections

The signal transfer from the function generator stimulus $\underline{V}_{STIM}$ to the relative output $\underline{V}_{PM}/\overline{V}_{PM}$ of the photomultiplier was determined by the product of

transfer functions $\underline{V}_{PM}/\overline{V}_{PM} = \underline{h}_{PM}\, S_{DYE}\, \underline{h}_{JM}\, \underline{h}_{CHIP}\, \underline{V}_{STIM}$. They are $\underline{h}_{CHIP} = (\underline{V}_S - \underline{V}_E)/\underline{V}_{STIM}$ from generator to chip, $\underline{h}_{JM}$ (or $\underline{h}_{FM}$) from chip to membrane, $S_{DYE} = (\underline{F}/F)/(\underline{V}_M - \underline{V}_J)$ from membrane voltage to relative fluorescence, and $\underline{h}_{PM} = (\underline{V}_{PM}/\overline{V}_{PM})/(\underline{F}/F)$ from relative fluorescence to relative photomultiplier signal. The product of transfer function $\underline{h}_{JM}$ (or $\underline{h}_{FM}$) with dye sensitivity S_{DYE} equals the relative modulation of fluorescence $\underline{F}/[F(\underline{V}_S - \underline{V}_E)]$ per chip voltage. It is obtained from dividing the measured signal $\underline{V}_{PM}/\overline{V}_{PM}$ by the transfer functions $\underline{h}_{PM}$ and $\underline{h}_{CHIP}$ and by the stimulus V^0_{STIM} according to Eq. 7.

$$\underline{h}_{JM}\, S_{DYE} = \frac{\underline{F}}{F(\underline{V}_S - \underline{V}_E)} = \frac{\underline{V}_{PM}}{\overline{V}_{PM}\, \underline{h}_{PM}\, \underline{h}_{CHIP}\, \underline{V}_{STIM}}. \quad (7)$$

The transfer function of the chips $\underline{h}_{CHIP}$ was obtained by monitoring the current across a 12 Ω resistance using a digital storage oscilloscope. It was modeled by a lowpass filter $\underline{h}_{CHIP}(f) = 1/(1 + i2\pi f\tau_{CHIP})$ with time constants $\tau_{CHIP} = 0.3$–1.2 μs, depending on oxide thickness and cell confluency. The transfer function of the photomultiplier h_{PM} was determined from AC illumination by a LED. It was fitted by a filter of fourth order $h_{PM} = [(1 + a_1P + b_1P^2)(1 + a_2P + b_2P^2)]^{-1}$ with $P = i\,f/f_B$ and $f_B = 615$ kHz with $a_1 = 0.7743$, $b_1 = 0.3890$, $a_2 = 1.3397$, and $b_2 = 0.4889$.

Data fit with plate contact model

The sheet resistance r_J was obtained as follows. Since the phase signal is not affected by the local dye sensitivity, we can fit the phase of the measured map $-\underline{F}/[F(\underline{V}_S - \underline{V}_E)] \propto \underline{h}_{JM}$ and $-\underline{F}/[F(\underline{V}_S - \underline{V}_E)] \propto \underline{h}_{FM}$ at the contact and in its surrounding using the plate contact model. We solved Eq. 5 on the lattice of the experimental pixels and fitted $\underline{h}_{JM}$ and $\underline{h}_{FM}$ to the phase map with varied sheet resistance r_J and given values of the capacitances. In a second step, the amplitude was fitted with a constant sensitivity $S_{DYE} < 0$. Crucial for a solution of Eq. 5 was the definition of the border of adhesion where the boundary condition $\underline{h}_J = 0$ holds. We defined it with a phase threshold of −45°. This approach was justified by the steep slope of the phase profile between 0° and −90° near the boundary (Fig. 2 *a*). Pixels at the periphery with phase values larger than the threshold were attributed to the upward bulging free membrane and are fitted with $\underline{h}_{FM}$. We visualized all experiments in terms of transfer functions $\underline{h}_{JM}$ and $\underline{h}_{FM}$, which means that the amplitude signal was scaled with a fitted global dye sensitivity S_{DYE}.

RESULTS

Erythrocytes

As a first example we studied the plasma membrane of human erythrocytes. These erythrocyte ghosts are free of intracellular structures that interfere with selective staining of the plasma membrane. They attach smoothly, with a hemispherical shape, to oxidized silicon coated with poly-L-lysine (Braun and Fromherz, 1997). We stained erythrocyte ghosts on chip type A with 10 nm thickness of oxide and imaged the fluorescence with 64 × 64 pixels each probing 0.17 μm × 0.17 μm (Fig. 3 *a*). The adhesion area is marked by a bright rim where the membrane bulges upwards. We applied an AC voltage between silicon and bath with amplitude $V^0_{STIM} = 2.5$ V and frequency $f = 25$ kHz. The modulation of fluorescence was recorded in amplitude and phase. As described in Materials and Methods, we corrected for delays of chip and photomultiplier amplifier and scaled with the sensitivity of the dye to infer the transfer functions $\underline{h}_{JM}$ and $\underline{h}_{FM}$. The signal quality was improved by a sliding average across 3 × 3 pixels with a final resolution of 0.5 μm.

The measured phase and amplitude maps of transfer functions $\underline{h}_{JM}$ and $\underline{h}_{FM}$ are shown in Fig. 3, *b*–*c*, and profiles are plotted in Fig. 3, *d*–*e*. The phase in the adhesion region exhibits a shallow trough with $\varphi(\underline{h}_{JM}) \approx -180°$ in the center and $\varphi(\underline{h}_{JM}) \approx -150°$ toward the periphery. In the surrounding, it jumps to $\varphi(\underline{h}_{FM}) \approx +20°$ where the signal is dominated by the upward bulging free membrane. The amplitude exhibits a broad maximum in the area of adhesion that decays to low values in the periphery. There it forms a narrow valley before it rises to higher values given by the amplitude of the free membrane.

The electrical properties of the contact were fitted from the phase map which revealed a sheet resistance $r_J = 1500 \pm 200$ MΩ with the given constants $c_S = 0.34$ μF/cm^2, $c_M = 1$ μF/cm^2, and $\beta_M = 0.5$. For illustration, phase and amplitude profiles are also plotted for a sheet resistance of $r_J = 500$ MΩ with dashed lines in Fig. 3, *d*–*e*. We estimate a systematic error of 20% based on uncertainties of 0.3 nm for the oxide thickness, 0.15 μF/cm^2 for the membrane capacitance, 0.05 for β_M, and 10% for the adhesion area. The characteristic frequency is $f_J = 6.4$ kHz, based on the adhesion area $A_{JM} = 30$ μm^2. The amplitude was fitted with a sensitivity $S_{DYE} = -2.5\%/100$ mV. The theoretical amplitude and phase are

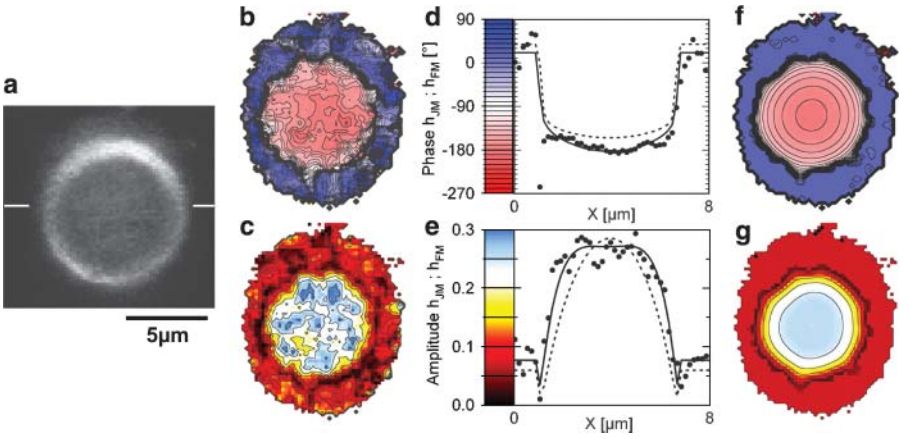

FIGURE 3 Fluorescence lock-in imaging of erythrocyte ghost. (*a*) Fluorescence image of erythrocyte ghost attached to a silicon chip with poly-L-lysine and stained with BNBIQ. (*b* and *c*) Measured phase and amplitude map of the transfer functions $\{\underline{h}_{JM}, \underline{h}_{FM}\}$ at $f = 25$ kHz. (*d* and *e*) Phase and amplitude profile across the attached ghost along the horizontal bar shown in *a*. The area contact model is fitted to the data with a sheet resistance $r_J = 1500$ MΩ (*solid line*) and plotted also for 500 MΩ (*dashed line*). (*f* and *g*) Theoretical phase and amplitude maps.

shown as solid lines in the profiles of Fig. 3, *d–e*, and as two-dimensional maps in Fig. 3, *f–g*.

HEK293 cells

HEK293 cells have been used for interfacing transistors and recombinant ion channels (Straub et al., 2001). They have a smooth membrane with low intrinsic ion conductance (Zhu et al., 1998). A large HEK293 cell on chip type A with 50 nm oxide is shown in Fig. 4 *a* with a resolution of 0.66 μm per pixel. Again a bright rim indicates where the membrane bulges upwards. We observed a distinct staining of the cytoplasm. Fig. 4, *b–d*, depicts phase and amplitude maps of the transfer functions $\underline{h}_{JM}$ and $\underline{h}_{FM}$ for $f = 125$ kHz and $V_S^0 = 3.0$ V. The phase map shows again two regions separated by a sharp boundary: a shallow trough in the adhesion area $\sim\varphi(\underline{h}_{JM}) \approx -150°$ and a surrounding with $\varphi(\underline{h}_{FM}) \approx +30°$. Fig. 4 *d* indicates a cupola of the transfer amplitude in the adhesion area. In contrast to the phase signal, the amplitude map looks rather erratic, suggesting that the effective dye sensitivity decreases due to enhanced inhomogeneous background of insensitive dye bound to intracellular structures.

We fit the phase map with a sheet resistance $r_J = 11$ MΩ with the constants previously used for erythrocyte ghosts. The theoretical phase profile is plotted in Fig. 4 *c*. To illustrate the accuracy, a profile with $r_J = 15$ MΩ is drawn with a dashed line. We infer f_J to be 76 kHz based on an adhesion area $A_{JM} = 470$ μm^2. We find a maximal dye sensitivity of $S_{DYE} = -6\%/100$ mV. Measurements with HEK293 cells of different shape yielded a mean sheet resistance of $r_J = 8.8 \pm 0.6$ MΩ ($N = 10$) on chips coated with fibronectin and slightly higher values of $r_J = 12.6 \pm 1.3$ MΩ ($N = 8$) on poly-L-lysine.

MDCK cells

MDCK cells are known for their high cell-cell resistance in confluent cultures (Lo et al., 1995). For that reason they are interesting candidates for bioelectronic devices. Using the same approach as with HEK293 cells, we found for single MDCK cells on polylysine almost the same features as for HEK293 cells (data not shown) with a similar sheet resistance of $r_J = 9.3 \pm 1$ MΩ ($N = 2$).

Rat neurons

The sheet resistance between nerve cells and silicon is crucial for the interfacing in neuroelectronic devices (Weis and Fromherz, 1997). We cultured rat neurons on type A chips with 50-nm oxide coated with poly-lysine under the conditions used for neuron-transistor junctions (Vassanelli and Fromherz, 1999). A neuron is shown in Fig. 4 *e* with a resolution of 0.42 μm, 3 × 3-binned to 1.2 μm. The phase and amplitude maps of the transfer function $\underline{h}_{JM}$ and $\underline{h}_{FM}$ for

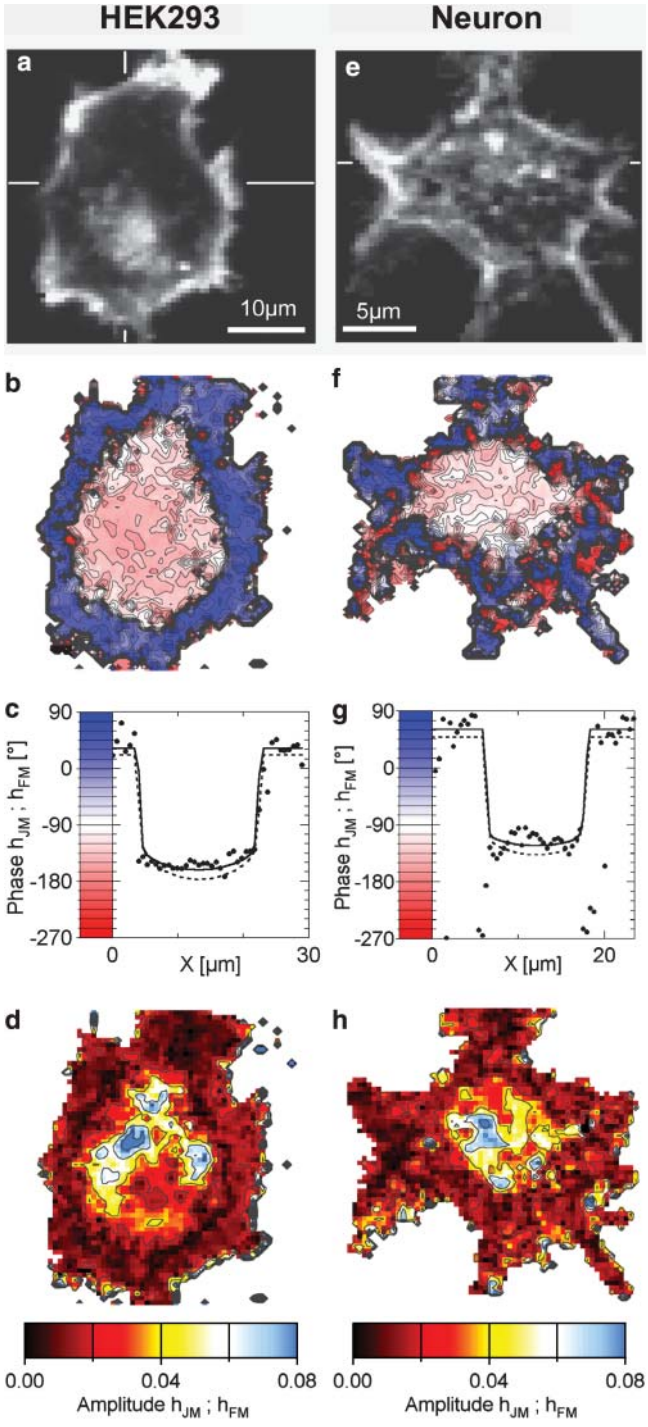

FIGURE 4 Fluorescence lock-in imaging of HEK293 cell (*left*) and rat neuron (*right*). (*a*) Fluorescence image of HEK 293 cell grown on fibronectin and stained with BNBIQ. (*b*) Measured phase map of the transfer function $\{\underline{h}_{JM}, \underline{h}_{FM}\}$ for HEK293 cell at $f = 125$ kHz. (*c*) Phase profile across HEK293 cell along the horizontal bar shown in *a*. The area contact model is fitted with a sheet resistance $r_J = 11$ MΩ (*solid line*) and plotted also for 15 MΩ (*dashed line*). (*d*) Amplitude map of the transfer function. (*e–h*) Analogous measurement of rat neuron grown on poly-L-lysine at $f = 125$ kHz, fitted with a sheet resistance of $r_J = 14$ MΩ (*solid line*) and plotted also for 23 MΩ (*dashed line*).

$f = 125$ kHz and $V^0_{STIM} = 2.5$ V are depicted in Fig. 4, *f–h*. The patterns of response are similar to HEK293 cells. The phase map shows two regions with a plateau in the adhesion area $\sim\varphi(\underline{h}_{JM}) \approx -120°$ and a surrounding with $\varphi(\underline{h}_{FM}) \approx +80°$. In the center of the cell, where the phase map is smooth, the amplitude signal is locally reduced. Those indentations correlate with high total fluorescence. The intracellular staining leads to an lower effective voltage sensitivity.

We fitted the phase map with a sheet resistance $r_J = 14 \pm 4$ MΩ for $c_S = 0.07$ μF/cm^2, $c_M = 1$ μF/cm^2, and $\beta_M = 0.5$ as shown in Fig. 4 *g* (*solid line*). We infer f_J to be 250 kHz based on an area $A_{JM} = 110$ μm^2. For illustration, a phase map was computed also for $r_J = 23$ MΩ as shown in Fig. 4 *g* (*dashed line*). The maximum dye sensitivity was found to be $S_{DYE} = -8\%/100$ mV.

Vertical scan of cell assembly

The presented method can be used to map cell-solid junctions in three dimensions. As an example, we performed a vertical scan through a bundle of HEK293 cells grown on chip type B with 50-nm-thick oxide. We can distinguish the attached membranes, the upper membranes, and the contacts of the cells as shown in the fluorescence image in Fig. 5 *a*. A section of phase and amplitude of the transfer function is shown in Fig. 5, *b–c*, for $f = 125$ kHz and an amplitude $V^0_{STIM} = 2.5$ V with a sliding average over 2×2 pixels (resolution 0.8 μm horizontal, 0.3 μm vertical). The amplitudes were scaled with $S_{DYE} = -6\%/100$ mV. We found that the phase is $\varphi(\underline{h}_{JM}) \approx -140°$ for the attached membranes and the lower parts of the cell-cell contacts. For the upper parts of the cell-cell contacts and the outer membranes we found $\varphi(\underline{h}_{FM}) \approx +20°$. There is a phase inversion between attached and free membrane at the periphery of the cell bundle as with individual cells. However, between two adjacent cells the phase change occurs at half the cell height. Further analysis reveals a linear drop in membrane potential along the cell-cell contact.

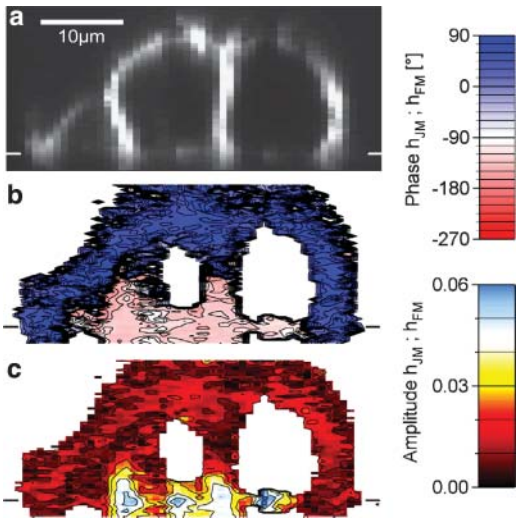

FIGURE 5 Fluorescence lock-in imaging across bundle of HEK293 cells. A bundle of HEK cells on fibronectin was stimulated by an AC voltage at $f = 125$ kHz. The response was recorded across a vertical section. (*a*) Fluorescence image of the vertical section. The position of the chip surface is indicated by a horizontal white line. (*b*) Measured phase map (color-coded) of the transfer function $\{\underline{h}_{JM}, \underline{h}_{FM}\}$ for the vertical section. (*c*) Amplitude map of the transfer function, scaled with an assumed dye sensitivity of $S_{DYE} = -6\%/100$ mV.

Voltage transients

Rectangular voltage pulses have been applied to silicon chips to achieve extracellular stimulation of nerve cells (Fromherz and Stett, 1995; Zeck and Fromherz, 2001). Optical recordings of the transient voltage in the attached membrane were reported for HEK293 cells (Braun and Fromherz, 2001). We tested the compatibility of AC stimulation and pulse stimulation for the cell already measured in Fig. 4, *a–d*. A train of voltage pulses was applied with a width of 4 μs, a period of 8 μs, and an amplitude of −6 V. Along the vertical white line in Fig. 4 *a*, we recorded the fluorescence over time with a resolution of 0.2 μs as shown in Fig. 6 *a*. Time traces from the attached membrane show a drop of fluorescence followed by a rise in the second half of the stimulation period. Toward the periphery, the transients fall

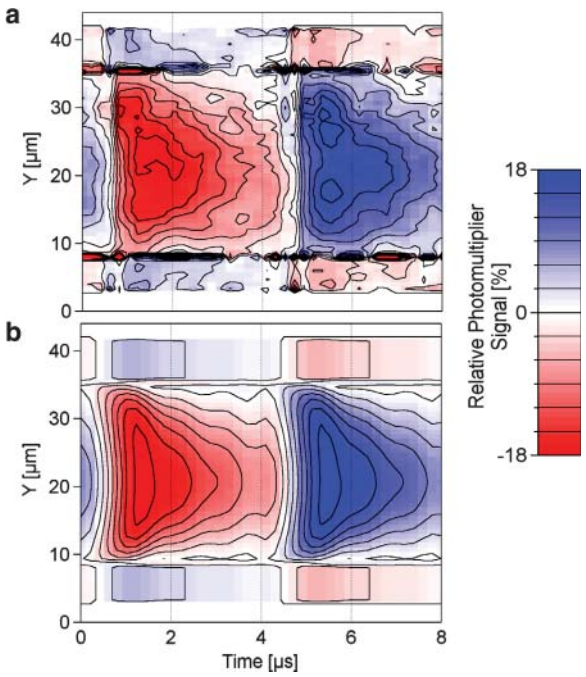

FIGURE 6 Fluorescent transients of HEK293 cell. The HEK293 cell shown in Fig. 4 *a* was stimulated with a train of negative rectangular voltage pulses at the chip (amplitudes $V^0_{STIM} = -6V$, durations and intervals 4 μs). (*a*) Relative change of photomultiplier response for one period along the vertical bar shown in Fig. 4 *a*. (*b*) Theoretical expectation based on the sheet resistance $r_J = 11$ MΩ inferred from the AC experiment.

off faster. The neighboring free membrane shows an inverted characteristic.

Using $r_J = 11$ MΩ as determined by the AC measurements, we computed the membrane potential as a function of time using the area contact model. It was convoluted with the transfer functions of chip and photomultiplier amplifier according to Eq. 7 (Braun and Fromherz, 2001) to obtain the expected fluorescence signal, as shown in Fig. 6 *b*, matching the measurement in all details. As expected, the AC measurements were sufficient to predict the behavior of the contact over time. It can be seen how the diffusive nature of the planar core-coat conductor leads to a faster falloff near the periphery.

DISCUSSION

Method

We pursued an electro-optical approach to analyze the seal characteristics of cells and tissue to a capacitive planar silicon electrode. The phase-sensitive lock-in technique improved signal quality and allowed us to measure membrane voltage maps at optical resolution. Several problems had to be solved. The setup had to be optimized for response times below microseconds by using a fast dye, by developing a fast chip with high fluorescence yield of attached cells, and by applying a fast fluorescence detector. A laser scanning microscope was necessary to differentiate the conflicting signals of attached and free membrane of cells.

Measurements with voltage-sensitive dyes are plagued by inhomogeneous sensitivities due to background staining. Since our technique relies only on the phase of the fluorescence signal, it can cope with large variations in voltage sensitivity (Fig. 4). Bleaching of the dye did not play a role and several scans of a cell were possible (Fig. 4, *a–d*, and Fig. 6). By increasing the stimulation voltage, large membrane potentials can be applied. Above 800 mV, cell death is indicated within half a minute by extracellular vesiculation, probably initiated by electroporation (Benz et al., 1979).

Seal resistance

Since we used the shape of each individual cell we could minimize systematic and statistic errors in the determination of the sheet resistance r_J. In cell-silicon systems the distance d_J between the insulating films of lipid bilayer and silicon dioxide is known from independent measurements by fluorescence interference contrast microscopy (Braun and Fromherz, 1998, 1997; Lambacher and Fromherz, 1996, 2002). So the sheet resistance r_J could be interpreted in terms of a specific resistance $\rho_J = r_J d_J$ in the cleft between cell and chip. For HEK293 cells on fibronectin we infer from $r_J = 11$ MΩ and $d_J = 50$ nm (data not shown) a specific resistance of $\rho_J = 55$ Ωcm, close to the bulk electrolyte $\rho_J = 75$ Ωcm. For rat neurons on polylysine we infer from $r_J = 14$ MΩ and $d_J =$ 60 nm (Braun and Fromherz, 1998) a specific resistance of $\rho_J = 84$ Ωcm, close to the bulk electrolyte $\rho_J = 115$ Ωcm. Similar relations were found for HEK cells on polylysine and single MDCK cells. We conclude that for all these cells, the cleft of ~50 nm between the lipid bilayer of the plasma membrane and silicon dioxide is filled with electrolyte from the surrounding culture medium. However, for erythrocytes on chips coated with polylysine, the sheet resistance of $r_J =$ 1.5 GΩ is higher by two orders of magnitude. Together with the close distance $d_J = 11$ nm (Braun and Fromherz, 1997), we infer a specific resistance $\rho_J = 1650$ Ωcm, which is 20-fold higher than $\rho = 75$ Ωcm of the bulk electrolyte.

We therefore see that a surface of cells, which flow freely like red blood cells, gives different seal characteristics than cells of brain, kidney, and epithelium which are usually embedded in a tissue. Erythrocytes have a glycocalix with a thickness of ~6 nm (Linss et al., 1991). We assume that here the narrow cleft induces polyelectrolyte effects in the glycocalix/polylysine layer which affect mobility and concentration of ions.

Relation to literature

Previous approaches to study the seal resistance of cells and electrodes lacked high spatial resolution. For that reason a global seal resistance R_J of the junction was considered (Regehr et al., 1988). A relation between global resistance and sheet resistance $R_J = r_J/5\pi$ was proposed (Weis and Fromherz, 1997). From Eq. 4 we obtain a modified relation $R_J = r_J/5.783\pi$. The area-specific conductance of the junction is $g_J = 5.783/r_J a_J^2$ for a radius a_J. A similar parameter $\alpha^2 = r_J a_J^2$ was used for confluent cell layers (Lo et al., 1995).

For erythrocytes on polylysine, $g_J = 132$ mS/cm^2 was reported from extracellular AC stimulation and transistor recording (Kiessling et al., 2000). With $a_J = 3$ μm the sheet resistance is $r_J = 0.5$ GΩ. For neurons on polylysine, $g_J \approx$ 1000 mS/cm^2 was determined by intracellular AC stimulation and transistor recording (Ephardt and Fromherz, 1993). With $a_J = 6$ μm the sheet resistance is $r_J = 16$ MΩ. These values are similar to our recordings, although they were obtained from a single transistor probe at an unknown location. Impedance measurements of confluent cell layers on gold were evaluated with $\alpha^2 = 49$ Ωcm^2 and 12.3 Ωcm^2 (Lo et al., 1995), $\alpha^2 = 324$ Ωcm^2 and 400 Ωcm^2 (Lo et al., 1995), $\alpha^2 = 4.84$–13.0 Ωcm^2 (Lo and Ferrier, 1998), and α^2 = 522 Ωcm^2 (Wegener et al., 2000). The given radii were a_J = 7–16 μm. The data of Lo and Ferrier (1998) lead to sheet resistances $r_J = 9.9$–26.5 MΩ, which are similar to our results. However, the high α^2 values of Lo et al. (1995) and Wegener et al. (2000) would lead to extremely high sheet resistances. The separation of sheet resistance and seal resistance between the cells may be ambiguous in the evaluation of global impedance measurements. By pulse stimulation and optical recording (Braun and Fromherz,

2001) with MDCK cell layers we observed a time constant of several milliseconds, as it is expected for a high seal resistance between the cells (data not shown).

CONCLUSIONS

By using a phase-sensitive lock-in, we imaged membrane voltage maps of cells stimulated by planar electrodes with micrometer and microsecond resolution in three dimensions. The measurements were explained by a planar core-coat conductor of the cell-electrode junction with the sheet resistance of the cleft between cell and substrate as the only fitting parameter. From the data we could infer the specific resistance in the cleft since the distances between cell and substrate were known from fluorescence interference measurements. For nerve cells, human embryonic kidney cells, and MDCK cells the specific resistance was indistinguishable from bulk electrolyte. Only for the special case of erythrocytes it was enhanced by a factor of 20.

In the present study we focused on electrical imaging of single cells to demonstrate the resolution of the method and to confirm microscopic details of electrical coupling between cells and electrodes. We find the novel method to be most useful to screen for better electrode coatings and to study other improvements of cell-electrode contacts. Such microscopic circuit information is crucial for both the stimulation and recording of electrical signals of nerve cells and neuronal assemblies. The microfluorometric approach is also able to reveal details of more complex geometries such as in tissue on electrodes. For example, details of voltage spread in brain slices could be revealed (Fromherz, 2002). In that case, two-photon excitation may be applied to achieve sufficient resolution in the tissue. A bottleneck here, however, is the staining with amphiphilic hemicyanines as their extracellular application is effective only a few cell layers deep. Cell-selective methods are required such as microinjection or genetic labeling, both not yet developed for these dyes.

We thank Bernd Kuhn for advice on the voltage-sensitive dye, Bernhard Straub for his expertise with backbonding of chips, Helge Vogl and Christian Figger for help in chip fabrication, Martin Maass from Olympus for the fruitful cooperation, and Raimund Gleixner and Hanna Salman for critical reading of the manuscript.

The project was supported by a generous grant of the Bundesministerium für Bildung und Forschung.

REFERENCES

Banker, G. A., and W. M. Cowan. 1977. Rat hippocampal neurons in dispersed cell culture. *Brain Res.* 126:397–425.

Benz, R., F. Beckers, and U. Zimmermann. 1979. Reversible electrical breakdown in lipid bilayer membranes: a charge-pulse relaxation study. *J. Membr. Biol.* 49:181–204.

Braun, D., and P. Fromherz. 1997. Fluorescence interference contrast microscopy of cell adhesion on silicon. *Appl. Phys. A.* 65:341–348.

Braun, D., and P. Fromherz. 1998. Fluorescence interferometry of neuronal cell adhesion on microstructured silicon. *Phys. Rev. Lett.* 81:5241–5244.

Braun, D., and P. Fromherz. 2001. Fast voltage transients in capacitive silicon-to-cell stimulation observed with a luminescent molecular electronic probe. *Phys. Rev. Lett.* 86:2905–2908.

Cohen, L. B., and B. M. Salzberg. 1978. Optical measurement of membrane potential. *Rev. Physiol. Biochem. Pharmacol.* 83:35–88.

Crank, J. 1975. Mathematics of Diffusion, 2nd Ed. Oxford University Press, New York.

Ephardt, H., and P. Fromherz. 1993. Fluorescence of amphiphilic hemicyanine dyes without free double-bonds. *J. Phys. Chem.* 97:4540–4547.

Fluhler, E., V. G. Burnham, and L. M. Loew. 1985. Spectra, membrane binding, and potentiometric responses of new charge shift probes. *Biochemistry.* 24:5749–5755.

Fromherz, P., A. Offenhäusser, T. Vetter, and J. Weis. 1991. A neuron-silicon junction: a Retzius cell of the leech on an insulated-gate field-effect transistor. *Science.* 252:1290–1293.

Fromherz, P., and C. O. Müller. 1993. Voltage-sensitive fluorescence of amphiphilic hemicyanine dyes in neuron membrane. *Biochim. Biophys. Acta.* 1150:111–122.

Fromherz, P., and A. Stett. 1995. Silicon-neuron junction: capacitive stimulation of an individual neuron on a silicon chip. *Phys. Rev. Lett.* 75:1670–1673.

Fromherz, P. 2002. Sheet conductor model of brain slices for stimulation and recording with planar electronic contacts. *Eur. Biophys. J.* 31:228–231.

Giaever, I., and C. R. Keese. 1991. Micromotion of mammalian cells measured electrically. *Proc. Natl. Acad. Sci. USA.* 88:7896–7900.

Graham, F. L., J. Smiley, W. C. Russel, and R. Nairn. 1977. Characteristics of a human cell line transformed by DNA from a human adenovirus type 5. *J. Gen. Virol.* 36:59–74.

Grinvald, A., A. Fine, I. C. Farber, and R. Hildesheim. 1983. Fluorescence monitoring of electrical responses from small neurons and their processes. *Biophys. J.* 42:195–198.

Gross, G. W. 1979. Simultaneous single unit recording in vitro with a photoetched laser deinsulated gold multielectrode surface. *IEEE Trans. Biomed. Eng.* 26:273–279.

Gross, D., L. M. Loew, and W. W. Webb. 1986. Optical imaging of cell membrane potential changes induced by applied electric fields. *Biophys. J.* 50:339–348.

Hibino, M., M. Shigemori, H. Itoh, K. Nagayama, and K. Kinosita, Jr. 1991. Membrane conductance of an electroporated cell analyzed by submicrosecond imaging of transmembrane potential. *Biophys. J.* 59: 209–220.

Kiessling, V., B. Müller, and P. Fromherz. 2000. Extracellular resistance in cell adhesion measured with a transistor probe. *Langmuir.* 16:3517–3521.

Kuhn, B., and P. Fromherz. 2003. Anellated hemicyanine dyes in neuron membrane: molecular stark effect and optical voltage recording. *J. Phys. Chem.* 107:7903–7913.

Lambacher, A., and P. Fromherz. 1996. Fluorescence interference-contrast microscopy on oxidized silicon using a monomolecular dye layer. *Appl. Phys. A.* 63:207–216.

Lambacher, A., and P. Fromherz. 2002. Luminescence of dye molecules on oxidized silicon and fluorescence interference contrast microscopy of biomembranes. *J. Opt. Soc. Am. B.* 19:1435–1453.

Linss, W., C. Pilgrim, and H. Feuerstein. 1991. How thick is the glycocalyx of human erythrocytes? *Acta Histochem.* 91:101–104.

Lo, C. M., C. R. Keese, and I. Giaever. 1995. Impedance analysis of MDCK cells measured by electric cell-substrate impedance sensing. *Biophys. J.* 69:2800–2807.

Lo, C. M., and J. Ferrier. 1998. Impedance analysis of fibroblastic cell layers measured by electric cell-substrate impedance sensing. *Phys. Rev. E.* 57:6982–6987.

Meyer, E., C. O. Müller, and P. Fromherz. 1997. Cable properties of dendrites in hippocampal neurons mapped by a voltage-sensitive dye. *Eur. J. Neurosci.* 9:778–785.

Pine, J. 1980. Recording action potentials from cultured neurons with extracellular microcircuit electrodes. *J. Neurosci. Meth.* 2:9–31.

Regehr, W. G., J. Pine, and D. B. Rutledge. Long-term in vitro silicon-based microelectrode-neuron connection. 1988. *IEEE Trans. Biomed. Eng.* 35:1023–1031.

Röcker, C., J. Heilemann, and P. Fromherz. 1996. Time-resolved fluorescence of hemicyanine dye: dynamics of rotamerism and resolvation. *J. Phys. Chem.* 100:12172–12177.

Rohr, S., and B. M. Salzberg. 1994. Multiple site optical recording of transmembrane voltage (MSORTV) in patterned growth heart cell cultures: assessing electrical behavior, with microsecond resolution, on a cellular and subcellular scale. *Biophys. J.* 67:1301–1315.

Schwoch, G., and H. Passow. 1973. Preparation and properties of human erythrocyte ghosts. *Mol. Cell. Biochem.* 2:197–218.

Straub, B., E. Meyer, and P. Fromherz. 2001. Recombinant maxi-K channels on transistor, a prototype of iono-electronic interfacing. *Nature Biotech.* 19:121–124.

Thomas, C. A., Jr., P. A. Springer, G. E. Loeb, Y. Berwald-Netter, and L. M. Okun. 1972. A miniature microelectrode array to monitor the bioelectric activity of cultured cells. *Exp. Cell Res.* 74:61–66.

Vassanelli, S., and P. Fromherz. 1999. Transistor probes local potassium conductances in the adhesion region of cultured rat hippocampal neurons. *J. Neurosci.* 19:6767–6773.

Wegener, J., A. Hakvoort, and H. J. Galla. 2000. Barrier function of porcine choroid plexus epithelial cells is modulated by cAMP-dependent pathways in vitro. *Brain Res.* 853:115–124.

Weis, R., B. Müller, and P. Fromherz. 1996. Neuron adhesion on silicon chip probed by an array of field-effect transistors. *Phys. Rev. Lett.* 76:327–330.

Weis, R., and P. Fromherz. 1997. Frequency dependent signal transfer in neuron transistors. *Phys. Rev. E.* 55:877–889.

Windisch, H., H. Ahammer, P. Schaffer, W. Müller, and D. Platzner. 1995. Optical multisite monitoring of cell excitation phenomena in isolated cardiomyocytes. *Pflugers Arch. Eur. J. Physiol.* 430:508–518.

Zeck, G., and P. Fromherz. 2001. Noninvasive neuroelectronic interfacing with synaptically connected snail neurons immobilized on a semiconductor chip. *Proc. Natl. Acad. Sci. USA.* 98:10457–10462.

Zhu, G., Y. Zhang, H. Xu, and C. J. Jiang. 1998. Identification of endogenous outward currents in the human embryonic kidney (HEK 293) cell line. *Neurosci. Meth.* 81:73–83.